ACS APPLIED MATERIALS & INTERFACES

Research Article

www.acsami.org

Synthesis of Hierarchically Porous SnO_2 Microspheres and Performance Evaluation as Li-Ion Battery Anode by Using Different Binders

P. Gurunathan, Pedda Masthanaiah Ette, and K. Ramesha*

CSIR−Network Institutes of Solar Energy (CSIR−NISE), CSIR Central Electrochemical Research Institute-Chennai Unit, CSIR-Madras Complex, Taramani, Chennai 600 113, India

Supporting Information

ABSTRACT: We have prepared nanoporous SnO_2 hollow microspheres (HMS) by employing the resorcinol-formaldehyde (RF) gel method. Further, we have investigated the electrochemical property of SnO_2−HMS as negative electrode material in rechargeable Li-ion batteries by employing three different binders—polyvinylidene difluoride (PVDF), Na salt of carboxy methyl cellulose (Na-CMC), and Na-alginate. At 1C rate, SnO_2 electrode with Na-alginate binder exhibits discharge capacity of 800 mA h g^{-1}, higher than when Na-CMC (605 mA h g^{-1}) and PVDF (571 mA h g^{-1}) are used as binders. After 50 cycles, observed discharge capacities were 725 mA h g^{-1}, 495 mA h g^{-1}, and 47 mA h g^{-1}, respectively, for electrodes with Na-alginate, Na-CMC, and PVDF binders that amounts to a capacity retention of 92%, 82%, and 8% . Electrochemical impedance spectroscopy (EIS) results confirm that the SnO_2 electrode with Na-alginate as binder had much lower charge transfer resistance than the electrode with Na-CMC and PVDF binders. The superior electrochemical property of the SnO_2 electrode containing Na-alginate can be attributed to the cumulative effects arising from integration of nanoarchitecture with a suitable binder; the hierarchical porous structure would accommodate large volume changes during the Li interaclation−deintercalation process, and the Na-alginate binder provides a stronger adhesion betweeen electrode film and current collector.

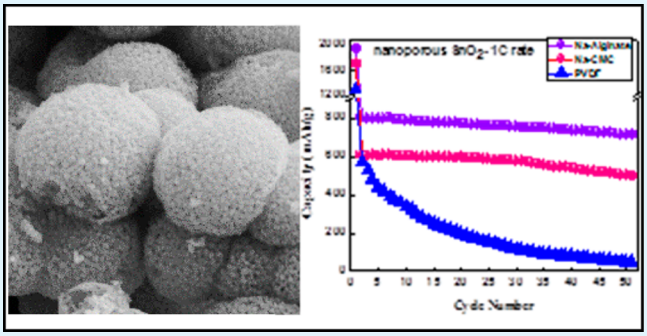

KEYWORDS: *SnO_2 hollow microspheres, lithium ion battery, anode, binder*

1. INTRODUCTION

The rechargeable Li-ion battery (LIB) technology has dominated the portable electronics market due to its high energy density[1] and is also becoming obvious choice for powering electric vehicles (EVs and HEVs) owing to their higher power capabilities.[2] LIBs also have the potential to be the storage device for renewable technologies such as solar and wind.[3−5] Currently graphite is used as anode in LIBs which has certain limitations, such as poor rate capability.[6] Hence Si and Sn have been considered as an alternate to graphite in LIBs due to their high theoretical capacity.[7,8] The gravimetric capacity of Si and Sn are respectively 3572 mA h g^{-1} and 992 mA h g^{-1}, which are much higher than that of graphite (374 mA h g^{-1}).[9−11] Similarly the volumetric energy density of Si (8322 mA h cm^3) and that of Sn (7254 mAhcm^3) are also significantly higher than that of graphite (818 mA h cm^3). However, use of Si and Sn as anode material was hampered by their poor cycle life due to the large volume change (~300%) associated with the lithiation/delithiation process.[12−15] The large volume change results in pulverization (mechanical degradation) of electrode causing loss of interparticle contact leading to deterioration of capacity retention. Several novel approaches have been developed to overcome this problem, such as coating carbon around nanoparticles or embedding nanoparticles in a carbon matrix.[16−18] But introduction of carbonaceous materials complicates electrode fabrication and also reduces active material loading.[19−21] One of the effective ways to overcome the issues of volume change during Li-insertion/deinsertion and prevent capacity degradation is by making use of hierarchically porous nanostructures such as hollow microspheres.[22−27] The hollow interior provides additional space to overcome strain associated with Li-insertion/deinsertion, thereby improving the cycling stability. The large surface area associated with hollow spheres provides better electrode−electrolyte contact area and thus offers shorter diffusion length and greater fraction of active sites. Such electrode architecture exhibits high capacity, higher rate capability, and good capacity retention in LIBs.

In addition to using nanoarchitectured materials for improving the capacity retention in the case of alloying electrodes such as Si and Sn, it has also been recognized that binders used for electrode processing also play an important

Received: May 10, 2014
Accepted: September 9, 2014
Published: September 9, 2014

role in improving cycle life.[28−32] Currently poly(vinylidene difluoride) (PVDF) has been widely used as the binder for fabrication of electrodes in LIBs. However, PVDF binder is expensive and also needs use of solvents such as *N*-methyl-2-pyrrolidone (NMP) which are very toxic.[33] Hence, in addition to developing active electrode materials, attention has to be devoted for the development of binders which are cheaper, less toxic, effective, and eco-friendly. Na salt of carboxy methyl cellulose (Na-CMC) has attracted attention as a binder due to its lower cost, water solubility, and nontoxicity.[33−37] Na-CMC has demonstrated promising characteristics; electrodes prepared using Na-CMC as binder have exhibited good cycling stability and capacity retention. Mazouzi et al. achieved good capacity retention over 700 cycles using Na-CMC binder for Si.[38] Recently, it has been shown that alginate, which is a natural polysaccharide extracted from brown algae, can be used as binder[32] for Si which exhibits remarkable capacity and long cyclability, better than when PVDF was used as binder.

In this work, we report the novel synthesis of hierarchically porous SnO_2 hollow microspheres (HMS) prepared by calcination of $SnCl_2$/resorcinol−formaldehyde gel resin in argon atmosphere, followed by heating the product in oxygen atmosphere. Further, we investigated electrochemical properties of SnO_2 HMS architecture by employing three different binders, viz., PVDF, Na-CMC, and Na-alginate. SnO_2 HMS along with Na-alginate binder exhibited higher capacity and good capacity retention over Na-CMC and PVDF. The results discussed here signify the importance of a binder especially when Si and Sn anodes are used in LIBs.

2. EXPERIMENTAL SECTION

2.1. Synthesis of Nanoporous SnO_2 Hollow Microspheres (HMS). The synthetic procedure followed here is similar to the one adopted for preparing NiO hollow spheres[39] and is shown as Scheme 1. In a typical synthesis, 1 g of $SnCl_2{\cdot}2H_2O$, 0.65 g of resorcinol, and 2 mL of 37% formaldehyde were dissolved in 20 mL of deionized water. This solution was vigorously stirred for half an hour to obtain a homogeneous solution and placed in a water bath at 80 °C for 4 h to produce $SnCl_2$/resorcinol−-formaldehyde (RF) gel. The gel was dried at 80 °C overnight. Subsequently, the dried gel was transferred to a tubular furnace and calcined at 700 °C for 2 h under flowing argon, followed by heating under oxygen atmosphere for 2 h at 700 °C to obtain nanoporous SnO_2 HMS. For comparing the electrochemical performance we also prepared nonporous/nonhollow SnO_2 particles (50−70 nm) by hydrolyzing $SnCl_2{\cdot}2H_2O$ in ammonia solution.

Scheme 1. Synthesis of SnO_2 Hollow Microspheres

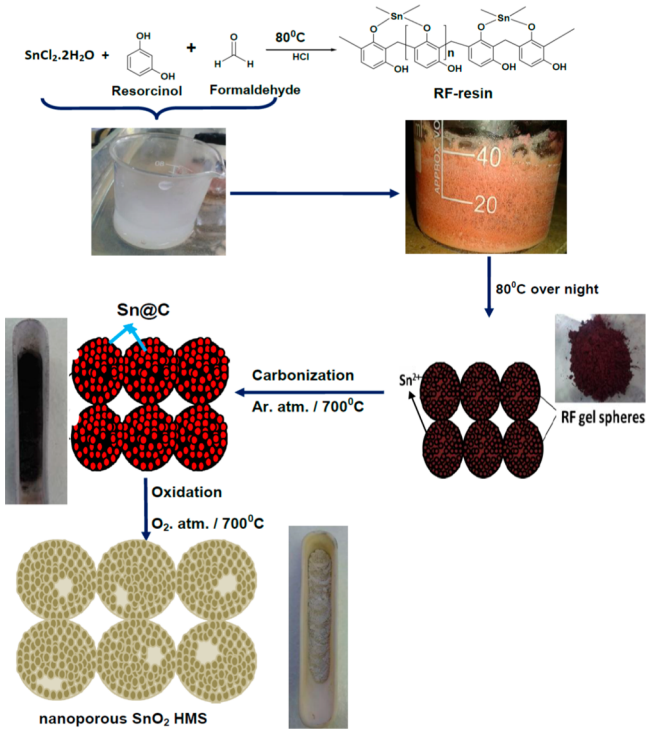

2.2. Material Characterization. Samples were analyzed by powder X-ray diffraction (PXRD) using Bruker D8 Advance Da Vinci diffractometer equipped with Cu Kα radiation source and a LynxEye detector. The morphology and size of the samples were characterized by a field emission scanning electron microscope (FESEM Carl Zeiss SUPRA55VP, Germany). Transmission electron microscopy studies were carried out with a Technai-20 G_2 microscope. Infrared spectra were recorded on an FT-IR spectrometer, Bruker Optick GmbH, with KBr pressed disks. Raman spectra were recorded using a Renishaw Laser Raman microscope. Thermogravimetric analysis (TGA) was carried out using a thermogravimetric analyzer (TG/DSC, Model STA449F3, NETZSCH Germany) with a heating rate of 5 °C min^{-1} in air.

2.3. Electrochemical Measurements. The electrochemical performance of SnO_2 HMS samples was evaluated galvaniostatically on CR2032 coin cells using a VMP3Z biologic multichannel battery testing system. Binders used in this study such as PVDF, Na-alginate, and Na-CMC are bought from Across organics. The working electrode was prepared by mixing active material (SnO_2 HMS), SP carbon, and a binder (Na-CMC or Na-alginate or PVDF), in a weight ratio of 70:20:10. It should be noted that deionized (DI) water was employed as the solvent for blending the electrode mixture when using Na-CMC or Na-alginate binders while *N*-methyl-2-pyrrolidone (NMP) was used as blending solvent for PVDF. The slurry thus prepared was coated on Cu foil and dried at 100 °C for 12 h under vacuum. The typical active material loading was 2 mg/cm^2. Cells were assembled in an Ar-filled glovebox by using Li foil as the counter electrode and reference electrode. A porous polypropylene film (Celgard) was used as separator, and 1 M $LiPF_6$ in ethylene carbonate (EC)/dimethyl carbonate (DMC)/diethyl carbonate (DEC) (2:1:2 in volume) was used as electrolyte. Cyclic voltametric (CV) measurements were carried out at a scan rate of 0.1 mV s^{-1} between 0.01−2.0 V at room temperature. Electrochemical impedance studies were performed over a frequency range of 400 kHz to 50 mHz at a discharged state of 0.01 V vs Li/Li^+ at room temperature.

3. RESULTS AND DISCUSSION

Figure 1 show X-ray diffraction (XRD) patterns of the product formed after initial carbonization of the gel under Ar atmosphere (Figure 1a) and that of the final product obtained after heating in oxygen atmosphere (Figure 1b). All the peaks in Figure 1a could be indexed to crystalline Sn (JCPDS card no. 86-2264) indicating formation of pure crystalline Sn metal (with uniform carbon coating) during calcination under argon. Figure 1b shows the XRD pattern for the final product after heating under oxygen atmosphere. All the diffraction peaks could be indexed on a tetragonal rutile structure of SnO_2 (JCPDS Card no. 41-1445). This confirms that Sn metal particles formed during initial heating under argon are oxidized to SnO_2 during the subsequent oxygen annealing process.

The morphology of SnO_2 particles was characterized by field-emission scanning electron microscopy (FESEM). Figure 2a shows the FESEM image of the Sn/C composite formed during heating the composite resin mixture under argon. A survey at low magnification (Figure 2b,c) reveals that the final sample annealed in oxygen is composed of hollow microspheres of size 700−800 nm with a relatively narrow size distribution. A high

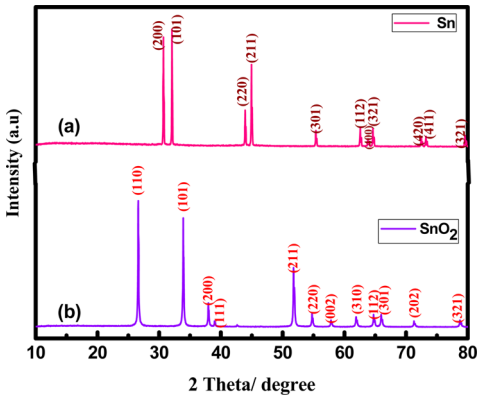

Figure 1. XRD patterns of (a) Sn/C composite prepared by calcination of $SnCl_2$/RF gel in argon atmosphere at 700 °C and (b) SnO_2 prepared by annealing Sn/C composite in oxygen atmosphere at 700 °C.

magnification FESEM image of microsphere (Figure 2d) clearly presents a hierarchical porous structure where a highly porous outer surface encloses a large hollow interior. Further, it can be seen that the sphere surface is made up of interconnected SnO_2 nanoparticles of 20 nm size leaving behind a porous network. Samples were grinded well before taking SEM/TEM images, which implies that the spherical morphology of SnO_2 is robust. Moreover, samples were intentionally ultrasonicated for a long duration in order to break or peel off a few spheres to confirm the presence of the hollow interior. As described in the later part, the unique hollow porous microsphere matrix will provide a large void space and mechanical support to release the strain induced during the alloying/dealloying of tin with lithium, thus preventing the pulverization of the electrode.

The morphology of SnO_2 spheres was further investigated by means of TEM as shown in Figure 3(a,b). Micrographs show almost spherical hollow structures. The porosity of the shell and its formation through aggregation of smaller particles is further supported by TEM images. Figure 3c shows the TEM image of some particles peeled off from the microspheres during ultrasonication. It can be seen that the sizes of these SnO_2 particles are about 20 nm. The SAED pattern (Figure 3d) taken on the SnO_2 particle shows high crystallinity of the sample.

Further, Raman and FT-IR spectroscopy were employed to characterize samples obtained from calcination of $SnCl_2$/RF gel under argon atmosphere (Sn/C composite) and after final oxygen annealing (SnO_2 HMS). Figure 4a shows Raman spectra for the Sn/C composite formed under Ar atmosphere. The spectra shows two broad peaks; the peak at 1585 cm^{-1} [G band] is an indication of sp^2 graphite carbon while the 1345 cm^{-1} [D band] corresponds to sp^3 disordered carbon.[40] Figure 4b shows Raman spectra of SnO_2 HMS formed after the final oxygen treatment. For rutile SnO_2 four active modes can be observed: A_{1g}, B_{1g}, B_{2g}, and E_g, out of which the A_{1g} mode is much stronger.[41] The observed peaks at 625 and 763 cm^{-1} can be assigned to A_{1g} and B_{2g} modes, respectively. The 498 and 680 cm^{-1} peaks are usually visible only in the case of SnO_2 nanocrystals as is the case here.[41]

Figure 5 shows FT-IR spectra of the products formed by heating SnO_2-RF gel in argon (Figure 5a) and by final oxygen annealing (Figure 5b). Peaks at 1000−1400 cm^{-1} are attributed to the C—OH stretching and O—H bending vibrations. Similarly the other observed peaks can be assigned: 1700 cm^{-1} (C═O stretching vibrations), 1610 cm^{-1} (C═C stretching), and 2920 cm^{-1} (stretching vibrations of O—H). Figure 5b shows the infrared spectrum recorded for SnO_2 hollow microspheres, which is consistent with that of the standard SnO_2.[42] The wide peak at 3417 cm^{-1} and weak peak at 1632 cm^{-1} are typical of the O—H vibrations due to the absorbed water. The bands at around 627 and 527 cm^{-1} can be attributed

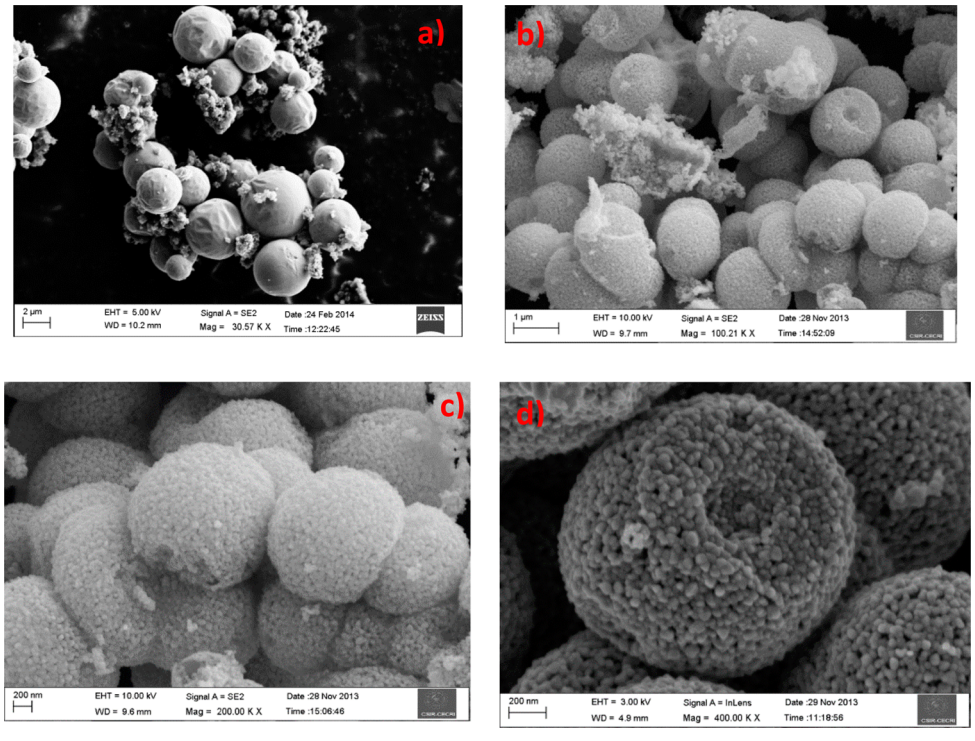

Figure 2. FESEM images of Sn/C composite (a) and nanoporous SnO_2 hollow microspheres at different magnifications (b−d).

dx.doi.org/10.1021/am502852x | ACS Appl. Mater. Interfaces 2014, 6, 16556−16564

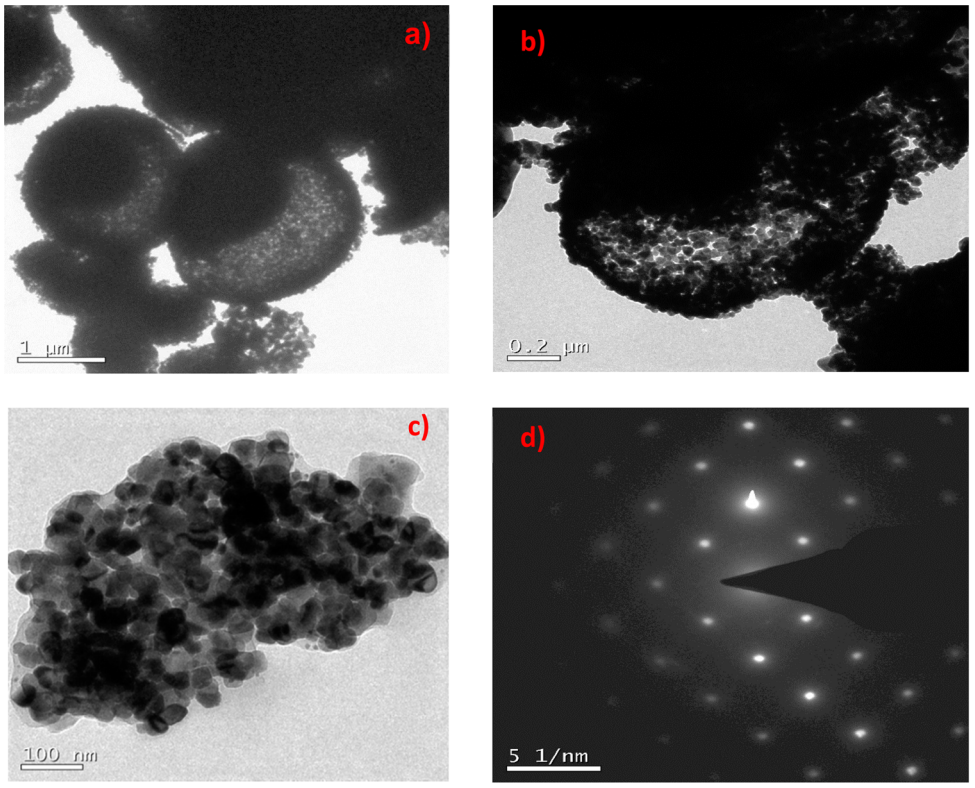

Figure 3. TEM images of nanoporous SnO_2 hollow spheres (a, b) and SnO_2 particles peeled off from the sphere surface (c); SAED pattern of SnO_2 particle (d).

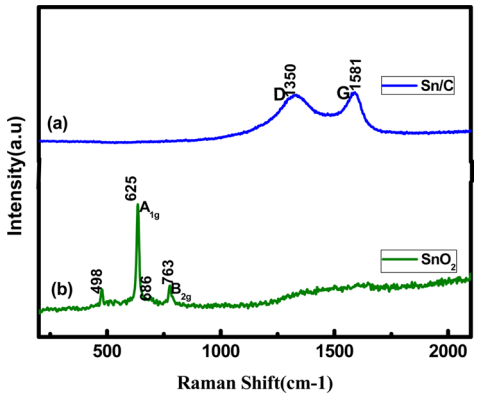

Figure 4. Raman spectra of (a) Sn/C composite and (b) SnO_2 microspheres.

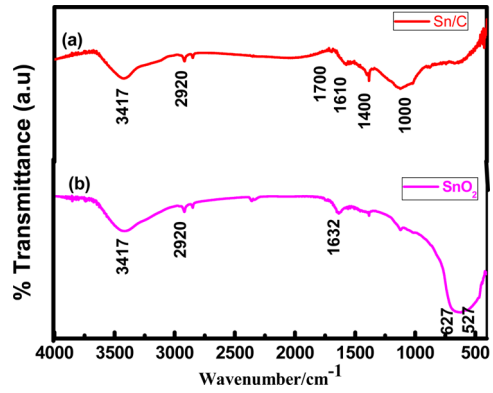

Figure 5. FT-IR spectra of (a) Sn/C composite and (b) nanoporous SnO_2 microspheres.

to the Sn—O stretching vibration and the O—Sn—O antisymmetric vibration.

In order to estimate carbon content and the thermal stability, thermogravimetric analysis (TGA) was carried out in air for Sn/C composite and SnO_2 HMS samples with a heating rate of 5 °C min^{-1}. While no weight loss is observed in the case of the SnO_2 HMS sample (Figure 6a), 50% weight loss was found for Sn/C sample (Figure 6b). The small weight loss below 100 °C was attributed to removal of moisture/adsorbed water. Almost no weight loss was observed for Sn/C composite at temperatures between 100 to 450 °C, demonstrating that the Sn/C composite is thermally stable in air up to 450 °C.[43,44] The weight loss from 450 to 550 °C is mainly due to carbon oxidation to CO_2.

We investigated the potential use of SnO_2 HMS as anode material for lithium ion batteries. Figure 7a shows the cyclic voltammogram (CV) of SnO_2−Na-alginate electrode for three cycles (first, second, and fifth) at a scan rate of 0.1 mV S^{-1} in the potential window 0.01−2.0 V. A reduction peak around 0.76 V is observed during the first cathodic scan and no longer appeared in the subsequent cycles which is attributed to the irreversible reduction of SnO_2 to Sn according to eq 1. The peak at 0.09 V can be attributed to formation of Li_xSn alloy as described by eq 2. Two corresponding anodic peaks are observed;[45] one is at about 0.53 V, which indicates the dealloying process of the Li_xSn alloy formed, and the other one is at about 1.2 V, which might indicate partial reversibility of reaction 1. In the second and next cycles, cathodic peaks appear at 0.91 and 0.62 V that can be ascribed to the formation of the solid electrolyte interphase[46] (SEI) and tin oxide reduction to metallic tin.[18]

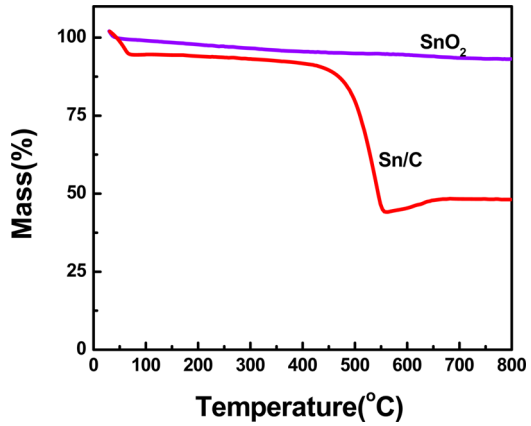

Figure 6. Thermogravimetric analysis (TGA) data for the Sn/C composite and nanoporous SnO_2 hollow microspheres heated in air at 5°/min.

$$SnO_2 + 4Li^+ + 4e^- \rightarrow Sn + 2Li_2O \quad (1)$$

$$Sn + xLi^+ + xe^- \leftrightarrow Li_xSn \quad (0 \le x \le 4.4) \quad (2)$$

In an electrode system the binder has the important role of holding active material and additives together.[47] Carbon based additives are used to provide electrical conductivity for the entire electrode. It is also essential that in addition to holding the active material and electronic additive together the binder should also provide a good ionic conductivity.[47] In the case of alloying electrodes such as Sn or Si, binders tend to fail from the above mentioned functionalities due to the large volume changes occurring during the Li intercalation/deintercalation process. So binders which can provide mechanical adhesion and ductility with tolerance to large volume change are highly desired for electrode systems such as Si, Sn.[32,47]

In order to highlight the importance of binder in the elctrochemical cycling of Sn based electrodes in LIBs, we have chosen three different binders for study, viz., Na-alginate, Na-CMC, and PVDF. Figure 7b–d shows the discharge/charge profile of nanoporous SnO_2 HMS between 0.01–1.2 V at 1C rate using Na-alginate, Na-CMC, and PVDF as binders. The initial discharge capacity of SnO_2 electrode with three different binders are in the following order: Na-alginate (1950 mA h g^{-1}) > Na-CMC (1700 mA h g^{-1}) > PVDF (1300 mA h g^{-1}). At the end of the first discharge the expected product is $Li_{4.4}Sn$. The first charging capacity is smaller than the first discharge capacity, for example, using alginate binder the first charging capacity observed is 998 mA h g^{-1}. The large irreversible capacity was ascribed mainly to irreversible reduction of SnO_2 to Sn in step 1. In the subsequent charge–discharge cycles it is Li_xSn which participates in the cycling, so compared to the first discharge, the second discharge capacity is less as it involves only the alloying process. From the second cycle onward the reversibility improved significantly. It could be noted that electrode with Na-alginate binder exhibits higher second discharge capacity of 800 mA h g^{-1}, compared to the electrodes with Na-CMC (605 mA h g^{-1}) and PVDF binders (571 mA h g^{-1}). After 50 cycles, discharge capacities of 725 mA h g^{-1}, 495 mA h g^{-1} and 47 mA h g^{-1} are obtained at 1C rate, respectively, for the electrodes with Na-alginate, Na-CMC, and PVDF binders with a capacity retention of 92%, 82%, and 8%.

We have also investigated rate capability of SnO_2 HMS at different discharge rates (0.2C to 5C), which is shown in Figure

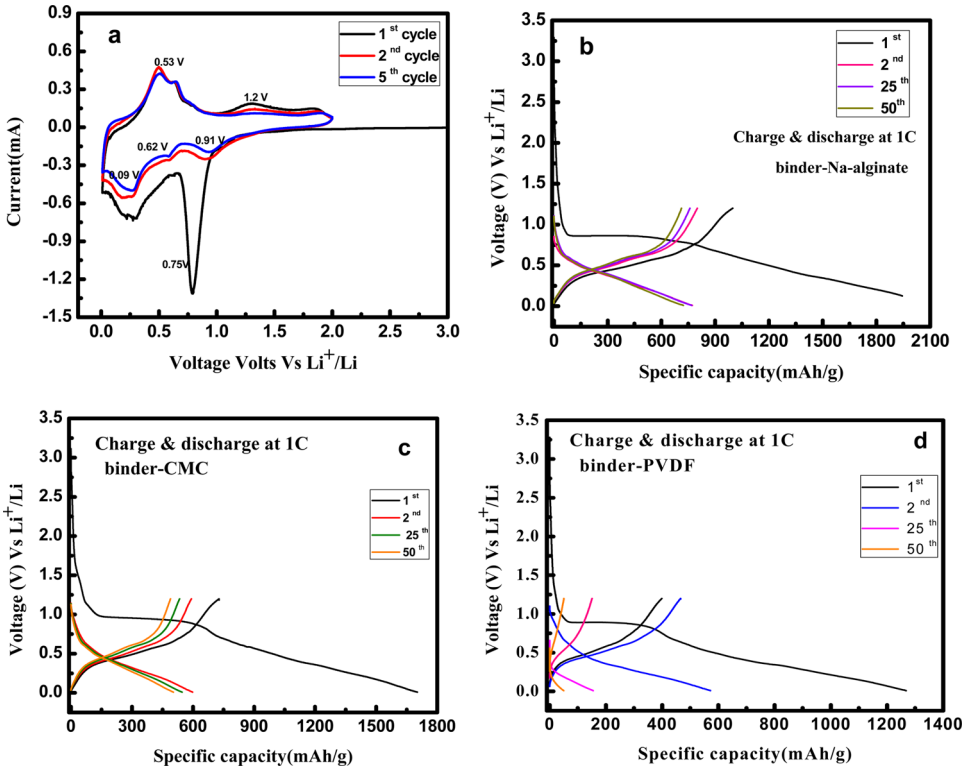

Figure 7. (a) Cyclic voltammogram (CVs) of nanoporous SnO_2 hollow microspheres within the voltage range of 2.0–0.01 V at 0.1 mV s^{-1} scan rate and (b–d) discharge/charge profile of SnO_2 electrode prepared using three different binders, (b) Na-alginate, (c) Na-CMC and (d) PVDF at 1C rate.

dx.doi.org/10.1021/am502852x | ACS Appl. Mater. Interfaces 2014, 6, 16556–16564

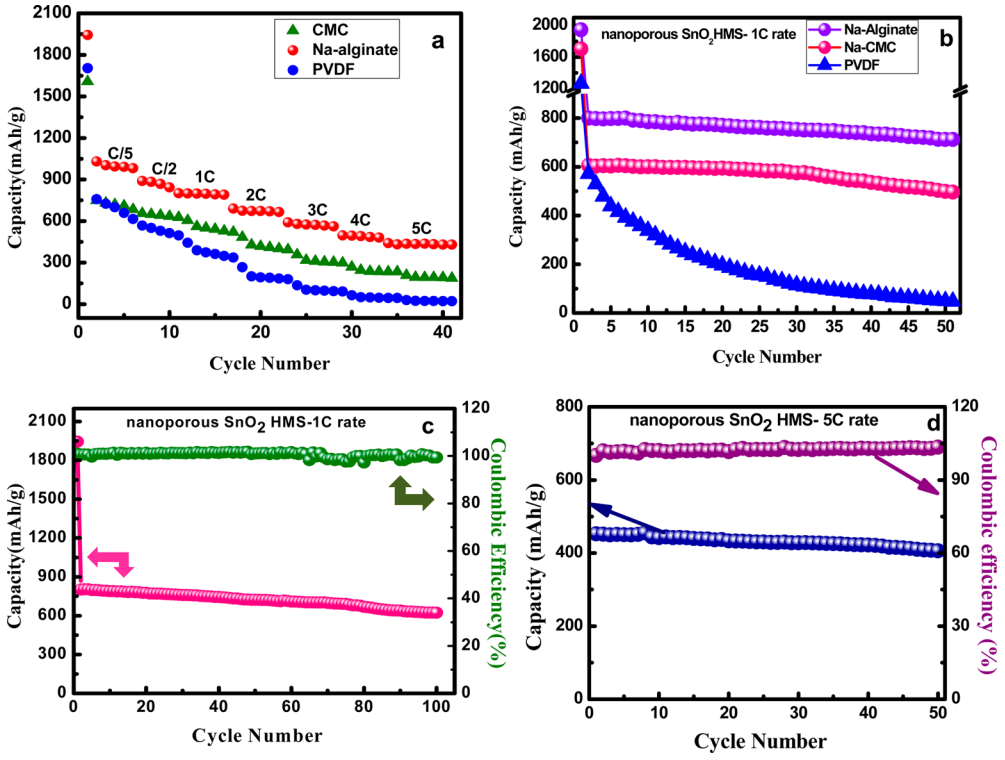

Figure 8. (a) Electrochemical cycling performance of SnO_2 hollow microspheres at different rates (0.2C−5C); (b) cycling performance of nanoporous SnO_2 hollow microspheres at 1C rate using different binders: Na-alginate, Na-CMC, PVDF; (c) long cycling (1C rate) and Coulombic efficiency of SnO_2 electrode using Na-alginate binder; and (d) high rate (5C) performance and Coulombic efficiency of SnO_2 hollow spheres using Na-alginate binder.

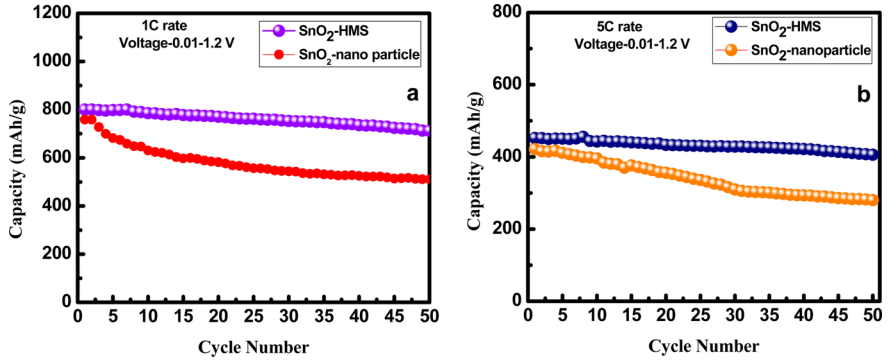

Figure 9. Comparison of electrochemical cycling performance of SnO_2 hollow microspheres and nonhollow SnO_2 nanoparticles at (a) 1C rate and (b) at 5C rates using Na-alginate as a binder.

8a. Electrodes prepared with PVDF showed poor rate capability at higher rates, for example, at 5C rate it showed capacity lower than 200 mA h g^{-1}, whereas Na-CMC electrode showed capacity of 400 mA h g^{-1} while Na-alginate electrode exhibited capacity of 550 mA h g^{-1}. Figure 8b compares long-term cycling performance of SnO_2 HMS electrodes consisting of the above-mentioned three binders. Capacity retention is poor for the electrode having PVDF binder. Out of two other binders used, the electrode having Na-alginate binder showed higher stable capacity (800 mA h g^{-1}) compared to that for Na-CMC (605 mA h g^{-1}), although both had good capacity retention. Figure 8c indicates good capacity retention for the SnO_2 electrode using Na-alginate as binder; at 1C rate after 100 cycles it showed capacity retention 79% and ∼635 mA h g^{-1} capacity with almost 100% Coulombic efficiency. Even at 5C rates after 50 cycles electrode with alginate binder exhibited good capacity retention (90%) with Coulombic efficiency of 100% (Figure 8d). Such a stable cycling performance was attributed to two factors, (i) the effective accommodation of volume changes during charge−discharge which is achieved through hollow and porous architecture and (ii) to the Na-alginate binder having a high modulus that holds active material and conductive additive together during the volume change. These results undoubtedly confirm the fact that Na-alginate binder could remarkably improve performance of SnO_2 anodes.

Further, we compared the electrochemical behavior of SnO_2 HMS with that of nonhollow SnO_2 nanoparticles using Na-alginate as binder (Figure 9a,b). These results support the fact that both the hollow nanostructured and the Na-alginate binder were responsible for superior electrochemical performance. It is evident that SnO_2 HMS showed better capacity retention compared to that of SnO_2 nanoparticles. SnO_2 HMS showed

dx.doi.org/10.1021/am502852x | ACS Appl. Mater. Interfaces 2014, 6, 16556−16564

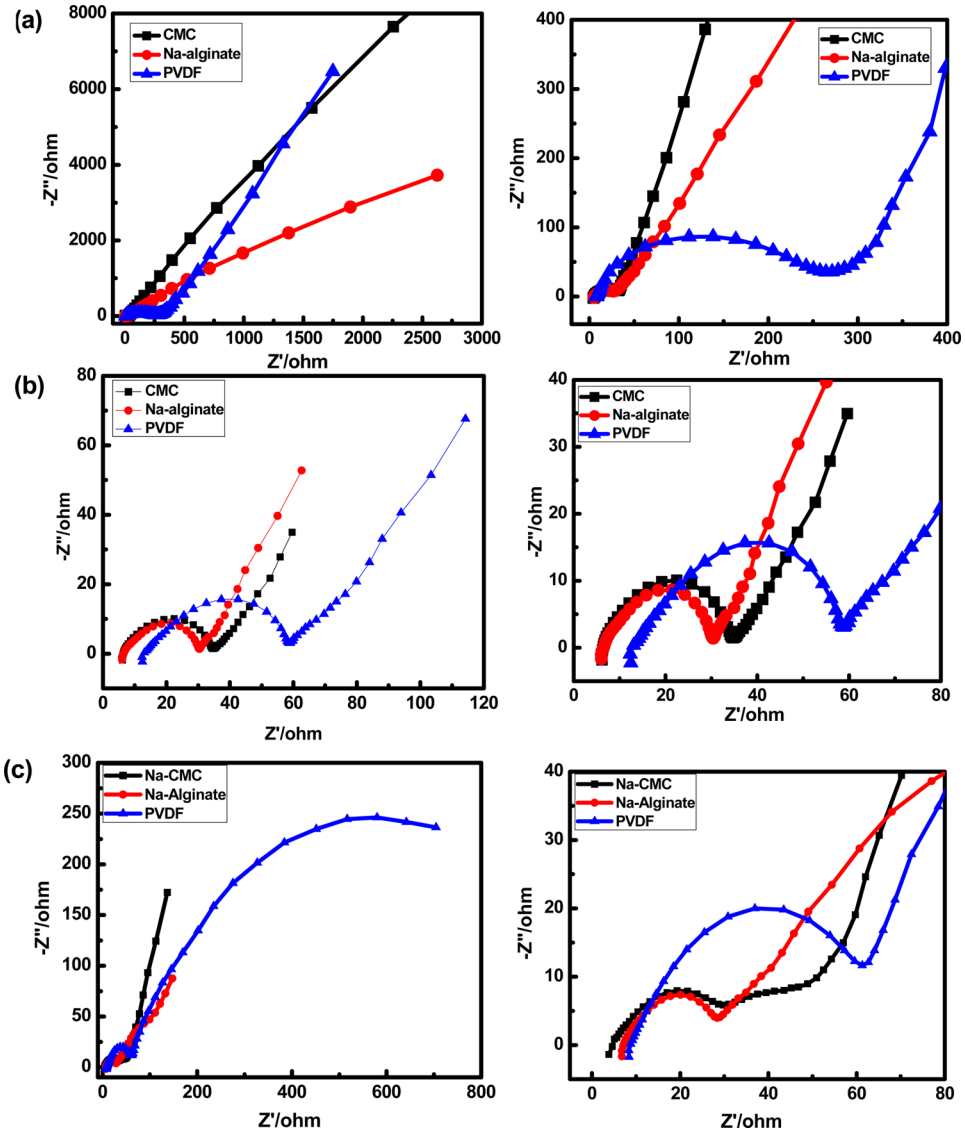

Figure 10. Electrochemical impedance spectra (EIS) of nanoporous SnO_2 hollow microspheres with three different binders—NaCMC, Na-alginate, and PVDF. (a) As prepared electrode, (b) after 2nd discharge, and (c) after 50th discharge cycle. Right hand side figures show enlarged (semicircle) region of the spectra.

capacity retention of 90% at 1C and 5C rates whereas SnO_2 nanoparticles showed 65% capacity retention after 50 cycles.

Electrochemical impedance spectroscopy (EIS) is used further to investigate electrode kinetics, rate capability, and other electrode characteristics. Figure 10 shows the Nyquist plots of the electrodes with three different binders, (a) as prepared electrode, (b) after two cyles, and (c) after completing 50 discharge−charge cycles. Impedance spectra show a slightly compressed semicircle in the medium frequency region which is commonly assigned to charge tranfer resistance (R_{ct}). For calarity, the expanded semicircle region is shown on the right-hand side of each plot. The R_{ct} for Na-alginate is much lower than that of Na-CMC and PVDF, indicating enhanced electrical conductivity of the Na-alginate containing electrode.[48]

It is evident that the as-prepared SnO_2 HMS electrode with Na-alginate binder[30,32] exhibits much better lithium storage capacity and cycling performance compared to the electrode with Na-CMC or PVDF binders. It is envisaged that carboxylic polar units present in the Na-alginate polymer chain ensure better interfacial interaction between the binder and the SnO_2 electrode material as well as a stronger adhesion between the electrode layer and the Cu substrate.[30] Moreover, due to the high viscosity the Na-alginate binder may prevent sedimentation and aggregation of SnO_2 and super-P carbon during electrode formulation, and this will enable uniform distribution of the electrical conducting network.[32] The most important criteria for a good binder are very weak binder−electrolyte interaction and that binder should assist in building a deformable but stable SEI on the electrode surface. The main issue with PVDF is its interaction with carbonate solvents due to which it shows swellability, resulting in change in mechanical properties. The Na-CMC and Na-alginate binders have shown the least interaction with electrolyte solvents.[32,49] Between Na-CMC and Na-alginate, the latter shows superior binder properties due to the difference in their functionalities. In Na-alginate each monomer has a carboxylic group which supports stronger hydrogen bonding interaction between binder and SnO_2 whereas Na-CMC has few and randomly distributed carboxylic groups in its polymeric structure. So two complimentary effects responsible for the good electrochemical

dx.doi.org/10.1021/am502852x | ACS Appl. Mater. Interfaces 2014, 6, 16556−16564

property of the SnO_2 HMS-alginate electrode system: (i) the hollow nanoarchitecture described here provides shorter diffusion length and good electrolyte percolation and an easy way to release the strain during intercalation/deintercalation, and (ii) the Na-alginate binder provides stronger adhesion between the electrode film and the current collector as well as uniform distribution of conducting networks. The synergy between these two effects is responsible for the superior electrochemical performance of nanoporous SnO_2 HMS-Na alginate electrode. At this point it is essential to demonstrate the stability of spherical hollow structures with respect to long charge−discharge cycling. FESEM images were recorded on the SnO_2 electrode (with Na-alginate binder) after completing 100 charge−discharge cycles (Figure S1 in the Supporting Information). FESEM images confirm that porous microspherical morphology of SnO_2 is retained even after prolonged electrochemical cycling.

4. CONCLUSION

In conclusion, we have successfully employed the RF gel method for the synthesis of SnO_2 HMS. Further, we have studied the electrochemical property of SnO_2 HMS as negative electrode material in LIB by employing three different binders—PVDF, Na-CMC, and Na-alginate. At 1C rate, the SnO_2 electrode prepared by using Na-alginate binder exhibited initial discharge capacity 800 mA h g^{-1}, higher than that when Na-CMC (605 mA h g^{-1}) and PVDF (571 mA h g^{-1}) were used as binders. After 50 cycles, the discharge capacities observed are 725 mA h g^{-1}, 495 mA h g^{-1}, and 47 mA h g^{-1}, respectively, for the electrodes prepared with Na-Alginate, Na-CMC, and PVDF binders, which amounts to capacity retentions of 92%, 82%, and 8% . After 100 cycles the SnO_2 electrode with alginate as binder delivered a capacity of 635 mA h g^{-1} with 79% capacity retention. These results show that the electrode prepared using Na-alginate binder presents better cycling performance and good rate capability than that with Na-CMC or PVDF binders. Interestingly, Na-CMC and Na-alginate binders are water-soluble, nontoxic, and also avoid use of any hazardous solvents. EIS results confirm that the SnO_2 electrode using Na-alginate as binder had a much lower charge transfer resistance and lower activation energy than for the electrodes with Na-CMC and PVDF binders. The superior electrochemical property can be attributed to the hollow SnO_2 nanoarchitecture which could accommodate large volume changes during the Li interaclation−deintercalation process and to the Na-alginate binder that provides a stronger adhesion betweeen electrode film and current collector. Notably these results highlight importance of a binder in preparing electrode, especially with alloying elecrodes such as Si and Sn. It also points out that, in addition to the efforts of improving electrode performance through developing nanomaterials, attention has also to be paid to developing suitable binders for Li ion battery electrodes.

■ ASSOCIATED CONTENT

Supporting Information

FESEM images of SnO_2 HMS-Na alginate electrode after 100 charge−discharge cycles. This material is available free of charge via the Internet at http://pubs.acs.org.

■ AUTHOR INFORMATION

Corresponding Author

*E-mail: ramesha.cecri@gmail.com.

Notes

The authors declare no competing financial interest.

■ ACKNOWLEDGMENTS

The authors thank Council of Scientific and Industrial Research (CSIR), India, for supporting this work under the TAPSUN programme. Mr. P. Gurunathan and Mr. Pedda Masthaniah Ette thank CSIR for providing financial support under the TAPSUN Project.

■ REFERENCES

(1) Marom, R.; Amalraj, S. F.; Leifer, N.; Jacob, D.; Aurbach, D. A Review of Advanced and Practical Lithium Battery Materials. *J. Mater. Chem.* **2011**, *21*, 9938−9954.
(2) Tarascon, J. M.; Armand, M. Issues and Challenges Facing Rechargeable Lithium Batteries. *Nature* **2001**, *414*, 359−367.
(3) Yang, Z.; Zhang, J.; Kintner-Meyer, M. C. W.; Lu, X.; Choi, D.; Lemmon, J. P.; Liu, J. Electrochemical Energy Storage for Green Grid. *Chem. Rev.* **2011**, *111*, 3577−3163.
(4) Dunn, B.; Kamath, H.; Tarascon, J. M. Electrical Energy Storage for the Grid: A Battery of Choices. *Science* **2011**, *334*, 928−935.
(5) Scrosati, B.; Garche, J. Lithium Batteries: Status, Prospects and Future. *J. Power Sources* **2010**, *195*, 2419−2430.
(6) Winter, M.; Besenhard, J. O.; Spahr, M. E.; Novák, P. Insertion Electrode Materials for Rechargeable Lithium Batteries. *Adv. Mater.* **1998**, *10*, 725−763.
(7) Liu, H. K.; Guo, Z. P.; Wang, J. Z.; Konstantinov, K. Si-based Anode Materials for Lithium Rechargeable Batteries. *J. Mater. Chem.* **2010**, *20*, 10055−10057.
(8) Zhang, W. J. Lithium Insertion/Extraction Mechanism in Alloy Anodes for Lithium-Ion Batteries. *J. Power Sources* **2011**, *196*, 877−885.
(9) Li, H.; Wang, Z. X.; Chen, L. Q.; Huang, X. J. Research on Advanced Materials for Li-Ion Batteries. *Adv. Mater.* **2009**, *21*, 4593−4607.
(10) Xie, Y.; Wu, C. Z. Design of Nano Architectured Electrode Materials Applied in New-Generation Rechargeable Lithium Ion Batteries. *Dalton Trans.* **2007**, 5235−5240.
(11) Zhang, T.; Gao, J.; Fu, L. J.; Yang, Y. L.; Wu, Y. P.; Wu, H. Q. Natural Graphite Coated by Si Nanoparticles as Anode Materials for Lithium Ion Batteries. *J. Mater.Chem.* **2007**, *17*, 1321−1325.
(12) Lou, X. W.; Wang, Y.; Yuan, C. L.; Lee, J. Y.; Archer, L. A. Template-Free Synthesis of SnO_2 Hollow Nanostructures with High Lithium Storage Capacity. *Adv. Mater.* **2006**, *18*, 2325−2329.
(13) Derrien, G.; Hassoun, J.; Panero, S.; Scrosati, B. Nanostructured Sn−C Composite as an Advanced Anode Material in High-Performance Lithium-Ion Batteries. *Adv. Mater.* **2007**, *19*, 2336−2340.
(14) Yu, Y.; Gu, L.; Zhu, C. B.; Van Aken, P. A.; Maier, J. Tin Nanoparticles Encapsulated in Porous Multichannel Carbon Microtubes: Preparation by Single-Nozzle Electrospinning and Application as Anode Material for High-performance Li-Based Batteries. *J. Am. Chem. Soc.* **2009**, *131*, 15984−15985.
(15) Yu, Y.; Gu, L.; Wang, C. L.; Dhanabalan, A.; Van Aken, P. A.; Maier, J. Encapsulation of Sn@Carbon Nanoparticles in Bamboo-like Hollow Carbon Nanofibers as an Anode Material in Lithium-Based Batteries. *Angew. Chem., Int. Ed.* **2009**, *48*, 6485−6489.
(16) Deng, D.; Lee, J. Y. Hollow Core−Shell Meso Spheres of Crystalline SnO_2 Nanoparticle Aggregates for High Capacity Li^+ Ion Storage. *Chem. Mater.* **2008**, *20*, 1841−1846.
(17) Lou, X. W.; Deng, D.; Lee, J. Y.; Archer, L. A. Preparation of SnO_2/Carbon Composite Hollow Spheres and Their Lithium Storage Properties. *Chem. Mater.* **2008**, *20*, 6562−6566.
(18) Chen, Y.; Huang, Q. Z.; Wang, J.; Wang, Q.; Xue, J. M. Synthesis of Monodispersed SnO_2@C Composite Hollow Spheres for Lithium Ion Battery Anode Applications. *J. Mater. Chem.* **2011**, *21*, 17448−17453.
(19) Wen, Z. H.; Wang, Q.; Zhang, Q.; Li, J. H. In Situ Growth of Mesoporous SnO_2 on Multiwalled Carbon Nanotubes: A Novel

Composite with Porous-Tube Structure as Anode for Lithium Batteries. *Adv. Funct. Mater.* **2007**, *17*, 2772−2778.
(20) Chen, G.; Wang, Z. Y.; Xia, D. G. One-Pot Synthesis of Carbon Nanotube@ SnO_2 − Au Coaxial Nanocable for Lithium-Ion Batteries with High Rate Capability. *Chem. Mater.* **2008**, *20*, 6951−6956.
(21) Chen, J. S.; Cheah, Y. L.; Chen, Y. T.; Jayaprakash, N.; Madhavi, S.; Yang, Y. H.; Lou, X. W. SnO_2 Nanoparticles with Controlled Carbon Nanocoating as High-Capacity Anode Materials for Lithium-Ion Batteries. *J. Phys. Chem. C* **2009**, *113*, 20504−20508.
(22) Lai, X.; Halpert, J. E.; Wang, D. Recent Advances in Micro-/Nano-Structured Hollow Spheres for Energy Applications: From Simple to Complex Systems. *Energy Environ. Sci.* **2012**, *5*, 5604−5618.
(23) Liu, J. L.; Li, W.; Manthiram, A. Dense Core−Shell Structured SnO_2/C Composites as High Performance Anodes for Lithium Ion Batteries. *Chem. Commun.* **2010**, *46*, 1437−1439.
(24) Lou, X. W.; Li, C. M.; Archer, L. A. Designed Synthesis of Coaxial SnO_2@Carbon Hollow Nanospheres for Highly Reversible Lithium Storage. *Adv. Mater.* **2009**, *21*, 2536−2539.
(25) Wang, Z.; Wang, Z. C.; Madhavi, S.; Lou, X. W. One-Step Synthesis of SnO_2 and TiO_2 Hollow Nanostructures with Various Shapes and Their Enhanced Lithium Storage Properties. *Chem. − Eur. J.* **2012**, *18*, 7561−7567.
(26) Chen, X.; Kierzek, K.; Wilgosz, K.; Machnikowski, J.; Chu, P. K.; Mijiowska, E. New Easy Way Preparation of Core/Shell Structured SnO_2@Carbon Spheres and Application for Lithium-Ion Batteries. *J. Power Sources* **2012**, *216*, 475−481.
(27) Han, B. S.; Jang, B.; Kim, T.; Oh, S. M.; Hyeon, T. Simple Synthesis of Hollow Tin Dioxide Microspheres and Their Application to Lithium Ion Battery Anodes. *Adv. Funct. Mater.* **2005**, *15*, 1845−1850.
(28) Bridel, S.; Azais, T.; Morcrette, M.; Tarascon, J. M.; Larcher, D. Key Parameters Governing the Reversibility of Si/Carbon/CMC Electrodes for Li-Ion Batteries. *Chem. Mater.* **2010**, *22*, 1229−1241.
(29) Fransson, L.; Eriksson, T.; Edstrom, K.; Gustafsson, T.; Thomas, J. O. Influence of Carbon Black and Binder on Li-Ion Batteries. *J. Power Sources* **2001**, *101*, 1−9.
(30) Magasinski, A.; Zdyrko, B.; Kovalenko, I.; Hertzberg, B.; Burtovyy, R.; Huebner, C. F.; Fuller, T. F.; Luzinov, I.; Yushin, G. Toward Efficient Binders for Li-Ion Battery Si-Based Anodes: Polyacrylic Acid. *ACS Appl. Mater. Interfaces* **2010**, *2*, 3004−3010.
(31) Guy, D.; Lestriez, B.; Guyomard, D. New Composite Electrode Architecture and Improved Battery Performance from the Smart Use of Polymers and Their Properties. *Adv. Mater.* **2004**, *16*, 553−557.
(32) Kovalenko, I.; Zdyrko, B.; Magasinski, A.; Hertzberg, B.; Milicev, Z.; Burtovyy, R.; Luzinov, I.; Yushin, G. A Major Constituent of Brown Algae for Use in High-Capacity Li-Ion Batteries. *Science* **2011**, *333*, 75−79.
(33) Lux, S. F.; Schappacher, F.; Balducci, A.; Passerini, S.; Winter, M. Low Cost, Environmentally Benign Binders for Lithium-Ion Batteries. *J. Electrochem. Soc.* **2010**, *157*, A320−A325.
(34) He, M.; Yuan, L. X.; Zhang, W. X.; Hu, X. L.; Huang, Y. H. Enhanced Cyclability for Sulfur Cathode Achieved by a Water-Soluble Binder. *J. Phys. Chem. C* **2011**, *115*, 15703−15709.
(35) Buqa, H.; Holzapfel, M.; Krumeich, F.; Veit, C.; Novák, P. Study of Styrene Butadiene Rubber and Sodium Methyl Cellulose as Binder for Negative Electrodes in Lithium-Ion Batteries. *J. Power Sources* **2006**, *161*, 617−622.
(36) EI Ouatani, L.; Dedryvere, R.; Ledeuil, J. B.; Siret, C.; Biensan, P.; Desbrieres, J.; Gonbeau, D. Surface Film Formation on a Carbonaceous Electrode: Influence of the Binder Chemistry. *J. Power Sources* **2009**, *189*, 72−80.
(37) Kim, G. T.; Jeong, S. S.; Joost, M.; Rocca, E.; Winter, M.; Passerini, S.; Balducci, A. Use of Natural Binders and Ionic Liquid Electrolytes for Greener and Safer Lithium-Ion Batteries. *J. Power Sources* **2011**, *196*, 2187−2194.
(38) Mazouzi, D.; Lestriez, B.; Roue, L.; Guyomard, D. Silicon Composite Electrode with High Capacity and Long Cycle Life. *Electrochem. Solid-State Lett.* **2009**, *12*, A215−A218.
(39) Huang, X. H.; Tu, J. P.; Zhang, C. Q.; Zhou, F. Hollow Microspheres of NiO as Anode Materials for Lithium-Ion Batteries. *Electrochem. Acta* **2010**, *55*, 8981−8985.
(40) Yu, X.; Yang, S.; Zhang, B.; Shao, D.; Dong, X.; Fang, Y.; Li, Z.; Wang, H. Controlled Synthesis of SnO_2@carbon Core-Shell Nano chains as High-Performance Anodes for Lithium-Ion Batteries. *J. Mater. Chem.* **2011**, *21*, 12295−12302.
(41) Shi, L.; Lin, H. Facile Fabrication and Optical Property of Hollow SnO_2 Spheres and Their Application in Water Treatment. *Langmuir* **2010**, *26*, 18718−18722.
(42) Xiao, L.; Li, J.; Li, Q.; Zhang, L. One-Pot Template-Free Synthesis, Formation Mechanism and Lithium Ions Storage Property of Hollow SnO_2 Microspheres. *J. Solid State Electrochem.* **2010**, *14*, 931−936.
(43) Hassoun, J.; Derrien, G.; Panero, S.; Scrosati, B. A. Nanostructured Sn−C Composite Lithium Battery Electrode with Unique Stability and High Electrochemical Performance. *Adv. Mater.* **2008**, *20*, 3169−3175.
(44) Liu, J.; Li, W.; Manthiram, A. Dense Core−Shell Structured SnO_2/C Composites as High Performance Anodes for Lithium Ion Batteries. *Chem. Commun.* **2010**, *46*, 1437−1439.
(45) Lou, X. W.; Chen, J. S.; Chen, P.; Archer, L. A. One-Pot Synthesis of Carbon-Coated SnO_2 Nanocolloids with Improved Reversible Lithium Storage Properties. *Chem. Mater.* **2009**, *21*, 2868−2874.
(46) Demir-Cakan, R.; Hu, Y. S.; Antonietti, M.; Maier, J.; Titirici, M. M. Facile One-Pot Synthesis of Mesoporous SnO_2 Microspheres via Nanoparticles Assembly and Lithium Storage Properties. *Chem. Mater.* **2008**, *20*, 1227−1229.
(47) Wu, M.; Xiao, X.; Vukmirovic, N.; Xun, S.; Das, P. K.; Song, X.; Olalde-Velasco, P.; Wang, D.; Weber, A. Z.; Wang, L. W.; Battaglia, V. S.; Yang, W.; Liu, G. Toward an Ideal Polymer Binder Design for High-Capacity Battery Anodes. *J. Am. Chem. Soc.* **2013**, *135*, 12048−12056.
(48) Chou, S. L.; Gao, X. W.; Wang, J. Z.; Wexler, D.; Wang, Z. X.; Chen, L. Q.; Liu, H. K. Tin/Polypyrrole Composite Anode Using Sodium Carboxy Methyl Cellulose Binder for Lithium-Ion Batteries. *Dalton Trans.* **2011**, *40*, 12801−12807.
(49) Zhao, X.; Cao, M.; Hua, C. Binder Strategy Towards Improving the Rate Performance of Nanosheet- Assembled SnO_2 Hollow Microspheres. *RSC Adv.* **2012**, *2*, 11737−11742.